Bound states in the *sp*-band gap of Ag/Au(111) thin films

A. Beckmann, M. Klaua, and K. Meinel
Max-Planck-Institut für Mikrostrukturphysik, D-4050 Halle, Weinberg 2, Germany
(Received 9 September 1992; revised manuscript received 22 February 1993)

Surface states and quantum-well states in thin metallic films are investigated within the framework of a nearly-free-electron (NFE) model and an effective-mass model by employing the Green's-function matching method. Applying the latter to Ag/Au(111), which is studied by angle-resolved photoemission, yields the edge parameters of the Ag *sp* band, viz., $E(L_2')=-0.35$ eV and the effective mass $m^*=-0.19$. The binding energies are obtained as a function of the film thickness. The NFE model with free-electron mass yields the best coincidence with the experimental data.

I. INTRODUCTION

In the past few years, investigations of bound states in metallic-layer systems have increasingly been carried out. High-resolution angle-resolved photoemission[1–3] enables local gaps in the bulk band structure to become accessible, which is a prerequisite to observe localized electronic states of surfaces and thin films.[4–9] The (111) surfaces of the noble metals are particularly interesting to study since the position of the Fermi level is located within an inverted *sp*-band gap with well-pronounced Shockley surface states with the *d* bands being well separated.

The evolution of the surface state in dependence on the film thickness yields information about the decay of the wave function. Ag/Au(111) (Ref. 5) and Ag/Cu(111) (Ref. 6) show a measurable shift of the surface-state binding energy which is unsymmetric with respect to the deposition of the complementary systems,[5] i.e., Au/Ag.

In addition, for Ag/Au(111) (Ref. 7) and Ag/Cu(111) (Ref. 8) quantum-well states have been obtained since in both cases the Ag band partially overlaps the local gap of the substrate. Here, the interfaces are expected to have a small effect on the quantum-well binding energy particularly for a high Ag deposition. However, comparing the papers of Miller *et al.*[7] with those of Mueller *et al.*[8] revealed differences larger than expected. The particular film structure is a probable reason for this discrepancy. The films should have a layer-by-layer structure of a well-defined thickness, a sharp interface without interdiffusion, and a high degree of structural perfection, i.e., they should have only few dislocations, stresses, or other deviations from ideal lattice structures. For the Ag/Cu(111) system, these presumptions are most problematic. Here, the misfit between the film and the substrate is relatively large (15%). Hence, a high degree of structural imperfections may be induced, even if the film had grown layerwise. For the Ag/Au(111) system, however, the misfit is almost vanishing (0.2%). Consequently, a layer-by-layer mode of film formation can be observed even at low temperatures without interdiffusion with the crystalline structure of the Ag film being almost ideal.[10–14] Thus, the Ag/Au(111) system seems to be more suitable for certain investigations of bound states in metallic-layer systems.

The motivation for reexamining the Ag/Au(111) system concerning the surface state and quantum-well states is based on our extensive experiences in the growth modes[10,14] and annealing behavior[12–14] of the Au/Ag(111) and Ag/Au(111) film-substrate systems enabling us to prepare two-dimensional homogeneous films of sharp interfaces and definite film thicknesses and therefore to correlate measured binding energies with film thicknesses in an unambiguous way. The experimental procedures[15] are briefly described in the next section. Further results of these experiments will be published elsewhere.[16] The present paper is mainly concerned with the theoretical interpretation of the binding energies of the observed localized states.

For studying states in a small region of the Brillouin zone it is advantageous to use parametrized models. These models may ensure the correct energies at the respective critical point. In this paper, the nearly-free-electron (NFE) two-band model and the effective-mass (EM) model are studied on the basis of the Green's-function matching method[17–21] to interpret localized states in thin films. The main equations following from that method are summarized in Sec. III as far as they are the basis of our calculations. Then it will be shown that for a homogeneous kinetic mass the phase rules of surface states[22–24] and quantum-well states[8] following from the multiple reflection approach are equivalent to the Green's-function matching eigenvalue equation.

The NFE model is commonly used to study *sp*-surface states of pure surfaces[17,20,22–24] as well as quantum-well states.[8,21] Both types of localized states in thin films can be described on the same basis. This simple model explains the different behavior of the binding energies of both states with respect to the film thickness.

For systems with large local gaps the effective-mass approach[25,26] is more satisfactory right from the beginning, since the expansion in k space uses the exact nondegenerate states at the L point, whereas in the NFE the base is degenerated and the gap-producing potential should be small for perturbation.

II. EXPERIMENTAL PROCEDURE

The photoemission experiments were carried out at the HASYLAB of the DESY in Hamburg using synchrotron

0163-1829/93/48(3)/1844(9)/$06.00 ©1993 The American Physical Society

radiation from the DORIS storage ring dispersed by a Seya-Namioka monochromator. The angle-resolved photoemission spectra were measured by an ADES 400 (VG) hemispherical analyzer with an acceptance angle of 2°.[15] In the range of photon energies from 9 to 24 eV the total energy resolution was <0.2 eV. The *p*-polarized radiation was incident in the $(1\bar{1}0)$ mirror plane at 45° with respect to the surface normal of the Ag(111) crystal. The electrolytically grown Ag(111) face was cleaned in the UHV chamber ($<5\times10^{-10}$ torr) by cycles of argon-ion bombardment (500 eV) and annealing to approximately 300 °C. Low-energy electron-diffraction (LEED) spots and the Ag(111) surface state in angle-resolved ultraviolet photoemission spectroscopy (ARUPS) were used to orient the crystal and to check the cleanness and well order of the surface.

The film thickness was determined by means of a quartz microbalance calibrated by means of Auger electron spectroscopy (AES) and TEM imaging of evaporated Au and Ag films. In addition, for the layer-by-layer growth the intensity of the surface-sensitive photoemission peaks of higher energies is proportional to the thickness with the proportionality factor abruptly changing whenever 1 monolayer is completed, which directly indicates the correctness of the determination of the film thickness with an uncertainty better than 5%.

III. FORMALISM

Localized states at surfaces, interfaces, and thin layers can be studied within continuous models by means of the surface Green's-function matching technique (SGFM).[17–21] For sharp interfaces between different potential regions, the matching planes are identified by boundaries and interfaces of the real physical system. The Green's function of the composite system is formulated in terms of the Green's functions of the subsystems. The bulk spectral properties of the components can be used to determine the parameters of the special model. The matching procedure for the interface projection G of the Green's functions $\mathbf{G}$ yields for one interface between media A and B (Ref. 18)

$$G^{-1}=-\lambda_A{}'G_A^{+}G_A^{-1}+\lambda_B{}'G_B^{-}G_B^{-1}\ , \tag{1}$$

and for two interfaces,[19] which bound the bulk (A), the thin film (B), and the vacuum region (C),

$$G^{-1}=-\begin{bmatrix}\lambda_A{}'G_A^{+}G_A^{-1} & 0\\ 0 & -\lambda_C{}'G_C^{-}G_C^{-1}\end{bmatrix}+\lambda_B\begin{bmatrix}{}'G_{Bll}^{-} & {}'G_{Blr}\\ -{}'G_{Brl} & -{}'G_{Brr}^{+}\end{bmatrix}\begin{bmatrix}G_{Bll} & G_{Blr}\\ G_{Brl} & G_{Brr}\end{bmatrix}^{-1}\ , \tag{2}$$

where the notation is explained by

$$G_{Blr}=\mathbf{G}_B(x=x_l,x'=x_r),\quad {}'G_{Bll}^{-}=\lim_{x=x_l+0}\frac{\partial\mathbf{G}_B(x,x_l)}{\partial x}\ . \tag{3}$$

The matrix indices l,r indicate the left and the right boundary with positions x_l and x_r, respectively. The present paper considers electronic states. Hence, λ is equivalent to the kinetic mass of the electron, $\lambda=(2m)^{-1}$, i.e., the kinetic-energy operator is $(p\,\lambda\,p)$. The conservation of the particle flux is fulfilled; for inhomogeneous kinetic mass,[27] however, there is a momentum exchange at the interface. Now, one needs the Green's functions for media A, B, and C or, at least, the ones projected onto the matching planes.

IV. THE NFE MODEL

The NFE model is used for both the substrate (region A) and the thin film (region B); it is chosen so that an inverse band gap is produced. It is well known[22] that surface states below the Fermi energy of metals can be obtained by taking into account the image potential. For the simple step potential, the surface-state energy lies above the Fermi energy; furthermore, there are no localized states of higher order (Rydberg states), which can be observed in inverse photoemission. However, the outer potential is expected to have a small effect on quantum-well binding energies, since details of the surface potential become less important for layers of some monolayers in thickness.

The Green's function is calculated by the Fourier transform, starting from the representation in the two-wave basis ($\langle x|k-g'\rangle, g'=0,g$),

$$\mathbf{G}_{gg'}(E)=\begin{bmatrix}-V_g\beta_+(\kappa) & V_g\\ V_g & -V_g\beta_-(\kappa)\end{bmatrix}^{-1}\ , \tag{4}$$

$$\beta_\pm=-[\lambda(\kappa\pm g/2)^2-E]/V_g\ , \tag{5}$$

leading to[28]

$$\mathbf{G}_M(x,x')=ie^{i\kappa|x-x'|}(2\lambda D^{1/2}\kappa V_g)^{-1}\{\cos(2\gamma)\cos[g(x-x')/2]+\cos[g(x+x')/2]+\sin(2\gamma)\sin[g|x-x'|/2]\}\ , \tag{6}$$

$$2\gamma=-i\ln(\beta_+)\ , \tag{7}$$

$$D=4EE_g+V_g^2\ , \tag{8}$$

$$\lambda\kappa^2=E+E_g-D^{1/2}\ . \tag{9}$$

κ,β,γ are analytical functions of E. Within the NFE model, the kinetic mass equals the effective mass at Γ. The band bottom parameter $E_g=\lambda(g/2)^2$ enables one to take into account the enlarged effective bandwidth owing to the hybridization with d bands via the effective mass at Γ. The Fourier component of the potential V_g is determined by the band gap Δ, which is $2|V_g|$. The values of the band edges L_1 and L_2' have been reported for Ag (Refs. 1 and 2) and Au.[3] For calculations, we use the values given in Table I. $E(L_2')$ of Ag is determined by our experiments as will be shown below. The matching planes are at $x=-d$ (half a monolayer to the inside, starting from the innermost atomic plane of the film) and $x=0$ (half a monolayer outwards the outermost atomic plane). The potentials at the matching planes and the effective masses m are assumed to change abruptly, whereas they are continuous within the regions (for region C, see Fig. 1). The expressions in (1) and (2) concerning A and B are determined from (6) as follows: for region A,

$$L_A \equiv {}'G_A^+ G_A^{-1} = q_A - \frac{g_A}{2}\tan\gamma_A \ , \qquad q_A = \mathrm{Im}(\kappa_A) \ , \tag{10}$$

and for region B,

$$\begin{bmatrix} {}'G_{B_{ll}}^- & {}'G_{B_{lr}} \\ -{}'G_{B_{rl}} & -{}'G_{B_{rr}}^+ \end{bmatrix} \begin{bmatrix} G_{B_{ll}} & G_{B_{lr}} \\ G_{B_{rl}} & G_{B_{rr}} \end{bmatrix}^{-1} = -iL_B \begin{bmatrix} \cot(\kappa d) & \cos(gd/2)/\sin(\kappa d) \\ \cos(gd/2)/\sin(\kappa d) & \cot(\kappa d) \end{bmatrix} , \tag{11}$$

$$L_B = -i\left[\kappa - i\frac{g}{2}\tan\gamma_B\right] . \tag{12}$$

κ, q, and g have the meanings of κ_B, q_β, and g_B, respectively. Note that the logarithmic derivative of the infinite B medium, L_B, is separated from a thickness-dependent part.

The parameters of the potential in region C are explained in Fig. 1. The logarithmic derivative at the surface is determined by the scattering of a free wave on the surface potential, i.e., one obtains

$$L_c \equiv {}'G_c^- G_c^{-1} = k_c \tan(\Phi_C/2) \ , \tag{13}$$

$$k_c = [\lambda_c^{-1}(E-V_1)]^{1/2} \ , \tag{14}$$

where Φ_C is the phase of the reflected wave with respect to a wave incoming from the pseudomedium C, which is characterized by the continuation of the constant value V_1 into the inside. The phases at $x=0$ and $x=x_1$ accumulate[23] since for $x>0$ the effective mass is homogeneous,

$$\Phi_C/2 = k_c x_1 + \arctan[L(x_1)/k_c] \ , \tag{15}$$

where $L(x_1)$ is the logarithmic derivative of the Whittaker function

$$L(x_1) = \left.\frac{W_{s1/2}'[(x-x_i)/4\lambda_c]}{W_{s1/2}[(x-x_i)/4\lambda_c]}\right|_{x=x_1} , \qquad s=[64\lambda_c(\phi-E)]^{-1/2} . \tag{16}$$

TABLE I. Band parameters.

	Ag	Au
L_2'	−0.35 eV	−1.10 eV
V_g	−2.1 eV	−2.25 eV
E_Γ	−7.21 eV	−9.0 eV
ϕ	4.74 eV	5.31 eV

ϕ is the work function. For numerical calculations it is sufficient to use the asymptotic expression[23] for $W_{s1/2}$. The parameters of the model, which have been specialized in different papers on surface states[20,22–24] are E_g (or the average bulk potential, respectively), the barrier bottom V_1 (see Fig. 1), and the image potential location x_i. For example, Smith[22] identified x_i with the geometric surface ($x_i=0$ in our coordinates), whereas Ortuño and Echenique[23] introduce the flat potential region V_1 in order to permit an adjustable phase shift. A general continuous potential model with the two free parameters x_i and V_1 was studied by Lenac *et al.*[24]

λ depends on x on a scale much larger than the atomic dimension. The energies of interest are near the band edges of A and B, but far below the vacuum level. Thus the $\lambda_A-\lambda_B-$ junction is useful even for larger film thicknesses, whereas the determination of λ_C seems to be more complicated. At energies far below the vacuum level, λ_C is expected to have approximately the value of the

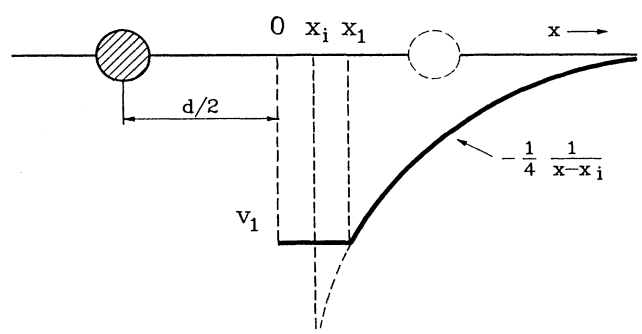

FIG. 1. Definition of the surface-potential parameters. x_i is the location of the image plane. V_1 is the constant potential of the surface region (for determination see text).

adjoining media A or B since the turning point of the wave is near the geometrical surface. However, we use $\lambda_C=\frac{1}{2}$ to ensure the electron to be asymptotically free near the vacuum level.

Unlike λ, the effective mass m^* of the lower-energy band at the L point has actually been determined in our photoemission experiments. In NFE approximation one obtains

$$\frac{1}{m^*}=-\frac{\lambda^2 g^2-2\lambda|V_g|}{|V_g|} . \tag{17}$$

The surface-potential parameters x_i, V_1, and ϕ strongly influence the binding energy of the surface state. Thus, these parameters will be discussed by means of the pure surfaces of Ag and Au, using the interface matching equation (1) before studying the thin-film case. The most natural way is to equalize V_1 with the inner potential of the outermost layer, i.e., either with that of Ag or of Au even for the thin-film case. The same assumption is applied to the work function. The parameter x_i will be fixed by the demand for reasonable binding energies for the surface states of both silver and gold. Then, of course, this value remains fixed for arbitrary coverages consisting of these components. Using the Green's-function matching method all types of localized states can be obtained. We will therefore analyze the eigenvalues in more detail.

V. SURFACE STATES

Three cases have to be distinguished. First, surface states on uncovered surfaces have energies within the band gap of the metal; second, true surface states on thin-film surfaces have energies in both band gaps of the substrate and of the thin film (Ag/Au); and third, artificial surface states exist within the band gap of the film but not in the gap of the substrate. For film thicknesses larger than the damping length, all kinds of surface states are in fact determined by the film. However, at smaller coverages, these states are thin-film-induced surface resonances. Here, it is sufficient to consider the two cases of true surface states since $L_2'(\mathrm{Ag})>L_2'(\mathrm{Au})$.

The eigenvalues of the localized states are determined by $\det(G^{-1})=0$. Thus, Eq. (1) generally describes a heterojunction between two regions of kinetic masses which are signified by λ_A and λ_C, since index B marks the film. The eigenvalue of the matching equation is consistent with the result of Morrow and Brownstein[27] who obtain a jump of the logarithmic derivatives at the inhomogeneous mass junction,

$$\lambda_A L_A-\lambda_C L_C=0 . \tag{18}$$

It is instructive to express the logarithmic derivatives by the scattering phases of free waves which are totally reflected for the energy of a bound state. This has already been used in Eq. (13). The reason for choosing free waves is the possibility of arbitrarily continuing the pseudomedium M beyond the physical domain.[19] Especially a flat potential can be used. As a result, Eq. (18) yields

$$\lambda_A\tan(\Phi_A/2)+\lambda_C\tan(\Phi_C/2)=0 , \tag{19}$$

which for the homogeneous mass ($\lambda_A=\lambda_C$) simplifies to the phase rule obtained from the multiple reflection approach[22]

$$\Phi_A+\Phi_C=2\pi n . \tag{20}$$

Especially for the NFE model, inserting (10) and (13) into (18) yields

$$\lambda_c k_c\tan(\Phi_C/2)=\lambda_A\left[q_A-\frac{g_A}{2}\tan(\gamma_A)\right] , \tag{21}$$

which is the result of Smith[22] for $\lambda_A=\lambda_C$.

For thin films one obtains

$$\coth(qd)=\frac{\lambda_A L_A\lambda_C L_C-\lambda_B^2 L_B^2}{(\lambda_A L_A-\lambda_C L_C)\lambda_B L_B} , \tag{22}$$

where (2) and (11) have been used. For thicknesses much larger than the decay length of the surface state, $qd\gg 1$, Eq. (22) leads to (18) with A replaced by B. Of course, if the surface state is totally localized within the layer, the wave function cannot probe the covered interface. Note that Eq. (22) is based on a discrete model with respect to the film thickness. Especially, the eigenvalues cannot be expanded in terms of d at $d=0$, which is in contrast to the approach of Hsieh and Chiang.[5]

VI. QUANTUM-WELL STATES

In that case the energy lies between L_2' (substrate) and L_2' (film), i.e., the waves may propagate through the film but not through the substrate. The eigenvalue condition yields

$$\cot(\kappa d)=i\frac{\lambda_A L_A\lambda_C L_C-\lambda_B^2 L_B^2}{\lambda_B L_B(\lambda_C L_C-\lambda_A L_A)} , \tag{23}$$

which presents a simple rotation of Eq. (22) in the complex κ plane. The right-hand side of (23) does not depend on the thickness d since all logarithmic derivatives L are thickness independent by definition. Hence, a quantization rule results with respect to κd including a certain phase. However, the interpretation by scattering phases is possible for a homogeneous junction ($\lambda_A=\lambda_B=\lambda_C$), where the phase rule[8] can be derived. In contrast to (20), the phases have to be defined with respect to the incoming and reflected Bloch waves of medium B. For example, in the NFE model

$$\Psi_k=e^{ikx}+\beta_+ e^{i(k-g)x} \tag{24}$$

is the wave incoming on C, i.e., Ψ_k^* is the reflected wave. Then, using the scattering phase, the total wave function for reflection on C may read as

$$\Psi_B=\Psi_k+e^{i\Phi_C}\Psi_k^* . \tag{25}$$

β_+ is defined in Eq. (8), whereas Φ_C is determined by the matching condition for the logarithmic derivatives at $x=0$. Together with the analogous formulation for the matching at $x=-d$, the following is yielded:

$$G^{-1}=i\lambda_B L_B \begin{bmatrix} \tan(\Phi_A/2)-\cot(\kappa d) & \dfrac{-\cos(gd/2)}{\sin(\kappa d)} \\ \dfrac{-\cos(gd/2)}{\sin(\kappa d)} & \tan(\Phi_C/2)-\cot(\kappa d) \end{bmatrix} , \tag{26}$$

$$\tan(\Phi_A/2)=iL_A/L_B , \tag{27}$$

$$\tan(\Phi_C/2)=-iL_C/L_B . \tag{28}$$

From (23), (27), and (28) one obtains

$$n=\frac{\kappa d}{\pi}+\frac{\Phi_A}{2\pi}+\frac{\Phi_C}{2\pi} , \tag{29}$$

which is the quantization rule for the Bloch wave vector keeping in mind $k=\kappa+g/2$.

VII. THE EM MODEL

Unlike NFE, here the basis is given by the eigenstates $\psi_0(k_0,x)$ and $\psi_1(k_0,x)$ belonging to the lower and upper bands[25,26] at the fixed point k_0, which here is the L point. The Green's function at $k=k_0+\kappa$ is given by

$$\mathbf{G}_{nn'}(\varepsilon)=\begin{bmatrix} \frac{1}{2}\kappa^2-\varepsilon & \kappa\rho \\ \kappa\rho & \frac{1}{2}\kappa^2-\varepsilon+\Delta \end{bmatrix}^{-1} , \tag{30}$$

which in real space yields[28,29]

$$\begin{aligned}\mathbf{G}_M(x,x')=-ie^{i\kappa|x-x'|}(2\kappa D^{1/2})^{-1}\{&[\alpha(\varepsilon)+\Delta]\psi_0(k_0,x)\psi_0^*(k_0,x') \\ &-\kappa\rho\,\mathrm{sgn}(x-x')[\psi_0(k_0,x)\psi_1^*(k_0,x')+\psi_1(k_0,x)\psi_0^*(k_0,x')] \\ &+\alpha(\varepsilon)\psi_1(k_0,x)\psi_1^*(k_0,x')\} ,\end{aligned} \tag{31}$$

$$\alpha(\varepsilon)=(\rho^2-\Delta/2)-D^{1/2} , \tag{32}$$

$$D=(\rho^2-\Delta/2)^2+2\rho^2\varepsilon , \tag{33}$$

$$\kappa^2/2=\alpha(\varepsilon)+\varepsilon . \tag{34}$$

Δ is the gap. The energy ε refers to the lower band edge L_2'. The effective mass at this point is connected with the momentum transfer element[26] ρ

$$\frac{1}{m^*}=1-\frac{2\rho^2}{\Delta} . \tag{35}$$

In comparison with NFE, the bandwidth or the effective mass at the Γ point, respectively, do not enter into m^*.

Using the symmetries of the inverse band-gap wave functions at the boundaries,

$$\psi_1=0, \quad \psi_0'=0 , \tag{36}$$

it is easy to rederive formulas (11), (22), (23), and (26)–(29) from (2) and (31) with

$$L_A=q_A+i\frac{q_A\rho_A}{\alpha_A+\Delta_A}\frac{\psi_1'(A)}{\psi_0(A)} , \tag{37}$$

$$L_B=-i\kappa+\frac{\kappa\rho_B}{\alpha_B+\Delta_B}\frac{\psi_1'(B)}{\psi_0(B)} . \tag{38}$$

Ratios ψ_1'/ψ_0 have to be determined by special band-structure calculations. In the NFE model, value $ig/2$ is obtained, which we use for numerical estimations. Summarizing the above, phase rules (20) and (29) are valid in EM in all cases since $\lambda_A=\lambda_B=\lambda_C=\frac{1}{2}$.

VIII. RESULTS AND DISCUSSION

Figure 2 shows angle-resolved normal-emission spectra obtained with $h\nu=9$ eV for various Ag film thicknesses evaporated on Au(111). The well-pronounced surface-state peak slightly below the Fermi level (energy zero) shifts with only a few monolayers of Ag deposition, whereas the weaker structures below move to higher energies over a large thickness region as long as they can be observed with more and more structures of that type occurring. These peaks are attributed to quantum-well states.[7] For this system, we have observed that possible deviations from ideal-film structures (polylayered film structure, first effects of interdiffusion) do not change the energy of the quantum-well states. Only the peak intensities are reduced.[16]

As explained above, the surface-potential parameters x_i and V_1 strongly influence the surface-state energies of the pure metals, whereas the band parameters of the Ag-*sp* band near the L point are directly obtained by fitting the energies of the first quantum-well state for large thicknesses. Since, on the other hand, the band bottom E_Γ is connected with these band parameters at the L point within the NFE model, with, furthermore, V_1 depending on E_Γ, we will discuss the *sp*-band parameters first.

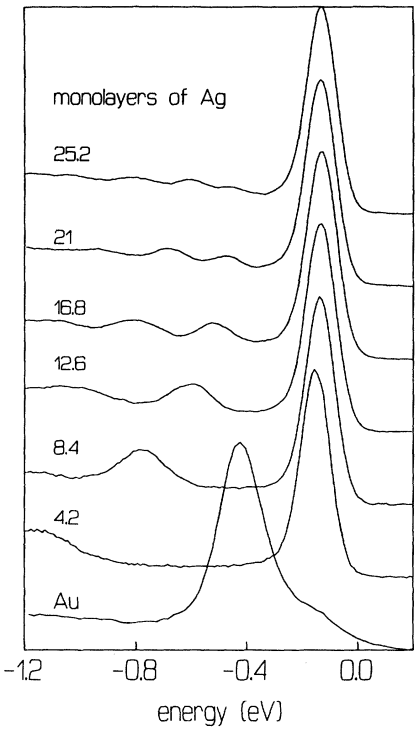

FIG. 2. Normal-emission spectra taken with a photon energy of $h\nu=9$ eV of Ag/Au(111) for various coverages as indicated.

At a fixed energy, the separation of the quantum-well series depends solely on the wave vector. Hence, the separation is unaffected by the interface potential which only causes a shift by means of the scattering phases. The accuracy of the k determination presupposes the exact determination of the film thickness as well as the homogeneity of the film. For inhomogeneous films, the thickness of contributing areas could be larger than the nominal one, especially in the region of the quantum-well onset (5–8 ML).

Our measurements yielded $L_2'(\mathrm{Ag})=-0.35$ eV and $m^*=-0.19$. These values are obtained by fitting the first quantum well for large thicknesses by a parabolic expansion with respect to k. A peak fit over a larger energy region would possibly yield a model-dependent value since higher-order terms in the k expansion of the energy could become important. For the NFE model, viz., Eq. (17), $m^*=-0.19$ corresponds to $\lambda_{\mathrm{Ag}}=0.49$, which is very close to the free-electron value. Qualitatively, the result agrees with Miller *et al.*[7] On the other hand, for the Ag/Cu(111) system Mueller *et al.*[8] obtained $m^*=-0.10$, corresponding to $\lambda=0.66$, which implies a broadening of the *sp* band via hybridization with *d* bands. However, the coincidence of the NFE value with the photoemission value should not be overestimated. For Cu(111), Kevan[25] finds that the NFE value for $|m^*|$ is at least a factor of 2 smaller than the experimental one. Furthermore, the value following from Kevan and Gaylord's measurements[4] is $\lambda_{\mathrm{Ag}}=0.41$, which is still smaller than ours. The discrepancy of the m^* values obtained for the systems Ag/Au(111) and Ag/Cu(111) remains problematic. It is open whether this discrepancy might be due to incorrect measurements of the film thickness, which is one of the most problematic parameters in film preparation. As explained in Sec. II, we are quite sure to have employed the correct data of film thickness in our experiments. The difference is probably caused by various interactions with inhomogeneities in both cases, such as, e.g., dislocations owing to the difference in film growth as well as nonlocal effects of the interfaces, i.e., the potential within B is influenced by the adjoining media.

TABLE II. Surface-potential parameters for various models.

	Ag	Au
NFE $m=1$	$V_1=-5.00$ eV $x_i=0.32$	$V_1=-5.62$ eV
EM	$V_1=-7.21$ eV $x_i=0.02$	$V_1=-9.00$ eV
NFE inhomogeneous model	$V_1=-7.21$ eV $x_i=-0.10$ $\lambda=0.66$	$V_1=-9.00$ eV $\lambda=0.75$

For the calculation, three cases are considered: (i) the NFE model with $\lambda_{\mathrm{Ag}}=\lambda_{\mathrm{Au}}=\frac{1}{2}$ (homogeneous NFE model), (ii) the EM model, (iii) the NFE model with the enlarged λ values corresponding to E_Γ (inhomogeneous NFE model) given in Table I. For all the three cases, the surface parameters are presented in Table II. V_1 refers to the Fermi level.

For determining x_i, the surface states of the pure Ag and Au (111) surfaces are studied. Figure 3 shows the dependence of the binding energy on x_i for the homogeneous NFE case. That model is favored by our experiments (Fig. 4). For further calculations we use the value

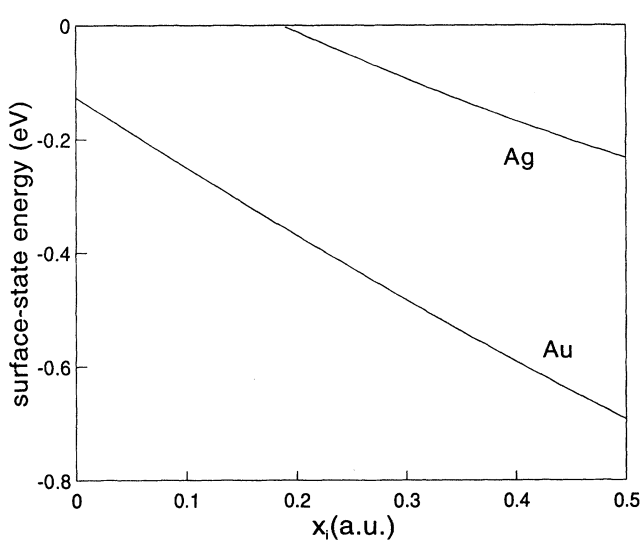

FIG. 3. The binding energies of the surface state of Ag and Au dependent on the image plane location x_i, calculated on the basis of the NFE model with $\lambda_{\mathrm{Ag}}=\lambda_{\mathrm{Au}}=0.5$. The energy zero is the Fermi level.

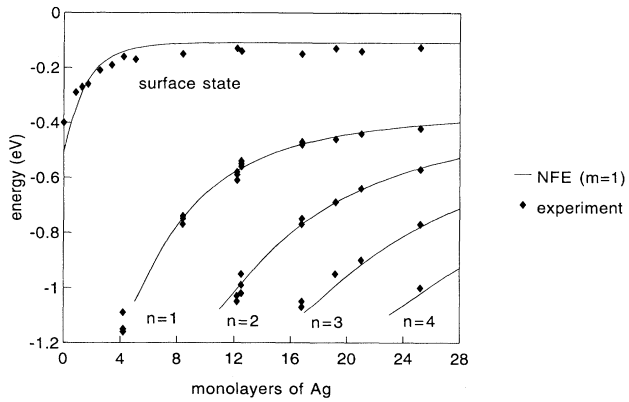

FIG. 4. Quantum-well and surface-state binding energies, measured by photoemission and calculated on the basis of the homogeneous NFE model. n labels the quantum-well numbers.

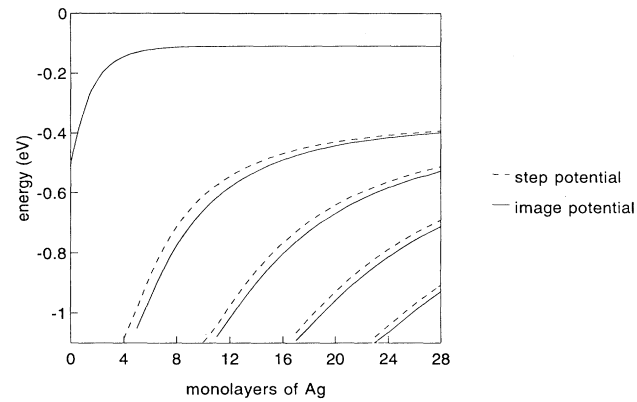

FIG. 6. Comparison of binding energies calculated for the NFE model with different surface potentials.

of $x_i = 0.32$, yielding reasonable surface-state binding energies for Ag and Au. A similar presentation for the inhomogeneous NFE model yields $x_i = -0.1$, whereas for the EM model $x_i = 0.02$ is obtained. The lower the potential V_1 is, the more the image plane has to approach the surface to yield the correct energies. The justification for our simple model relies on the correct description of the thickness dependence of the energies. The calculations cannot yield the value of x_i. It is interesting that x_i strongly depends on the inner potential, but has almost the same value for Ag and Au. Hence, it is justified to take the same value for both.

Figure 5 compares the quantum-well spectra calculated for the three cases. The agreement between the EM model and the homogeneous NFE model is excellent. The λ_{Ag} values are almost the same and the energy region of interest is small enough for the band to be parabolic. The surface-state binding energies of pure Au are too large in all the cases, especially in the inhomogeneous model. The separation at a fixed energy increases with the mass decreasing, according to $\Delta L \propto |m^*|^{-1/2}$.

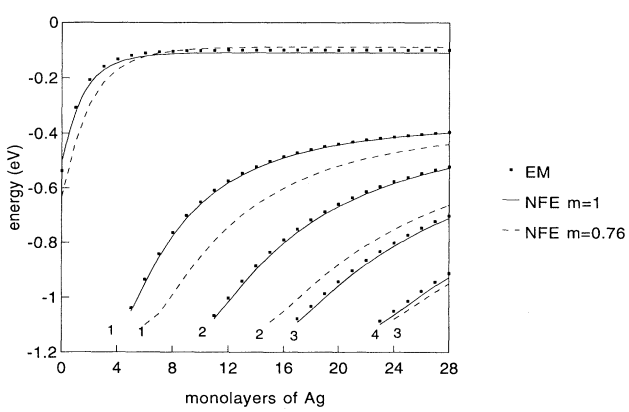

FIG. 5. Comparison of binding energies calculated for the EM model, the homogeneous NFE model, and the inhomogeneous NFE model.

Figure 6 shows that the surface potential indeed has a small effect on the quantum-well energies, whereas the surface state strongly depends on the surface potential. For the step potential, there is no surface state below the Fermi energy, independently of the layer thickness.

The different contributions in Eq. (29) to the phase quantum number are demonstrated in Fig. 7 for $d = 20$

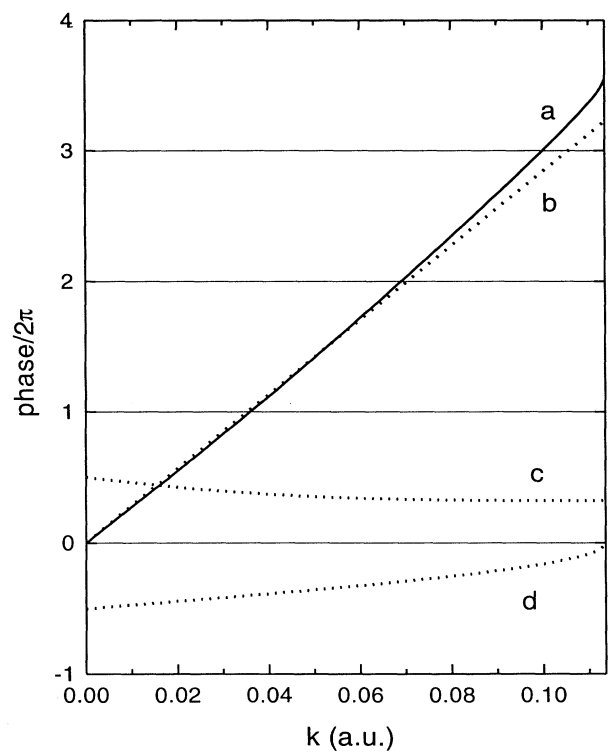

FIG. 7. The contributions of Eq. (29) to the normalized phase for $d = 20$ ML, as a function of the wave vector, calculated for the homogeneous NFE model. (a) Sum of all contributions, i.e., the right-hand side of (29). (b) The linear contribution. (c) The phase of surface scattering $\Phi_C/2\pi$. (d) The phase of scattering on the interface $\Phi_{Au}/2\pi$.

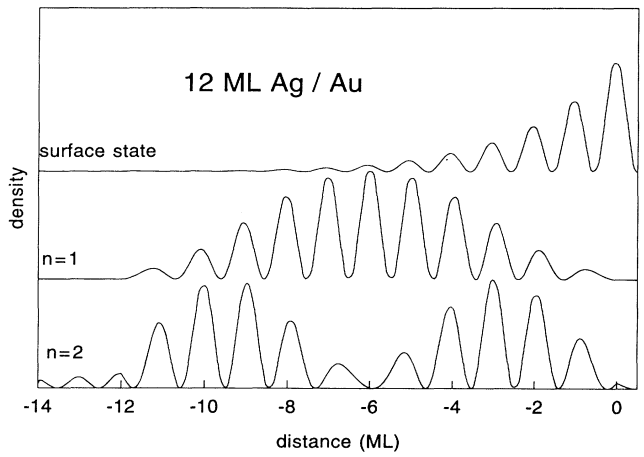

FIG. 8. The density of the bound states, calculated on the basis of the homogeneous NFE model for $d=12$ ML Ag/Au(111). The distance refers to the surface in units of 1 ML of silver.

ML. Note that (20) and (29) are not valid for model 3 since the premise was a homogeneous junction. For clarity, the energy dependence of the phases is transformed to the film wave vector k via the band dispersion. $k=0$ is the band edge of Ag, whereas $k=0.11$ indicates the band edge of Au, i.e., $E(L_2')=-1.1$ eV. The eigenvalues of the wave number are defined by the points at which the sum curve has integer values. At $L_2'(\mathrm{Ag})$, the two phases cancel each other. Thus, the linear contribution dominates over a wide range. The same calculation using the step potential shifts the surface phase slightly above curve (c) in Fig. 7 which, however, is sufficient to explain the different results of both models in Fig. 6. It is easy to prove that in our models Φ_{Au} vanishes like the square root of the energy measured from the band edge as it generally should be the case.[8]

Figure 8 shows the density of electrons of the localized states for $d=12$ ML. The functions are normalized to their maximum value. The amplitude of the quantum-well states agrees with the result of Jaskolski, Velasco, and Garcia-Moliner.[21] The surface state is entirely localized within the layer. The substrate no longer influences the surface state. Looking at the substrate region ($x<-12$), it turns out that the quantum-well state $n=1$ is more localized on the film region than the state $n=2$, owing to the fact of the energy of $n=2$ being closer to $L_2'(\mathrm{Au})$.

IX. CONCLUSIONS

The main purpose of the present paper is to show that Shockley-type surface states and quantum-well states in thin films belong to different eigenvalues of the same Green's-function matching equation. The obvious conditions for their existence are the following: (i) The film should have an inverted band gap to guarantee that there is a surface state; (ii) the occupied *sp* band partially overlaps the local band gap of the substrate. Both types of localized states are observed in the system Ag/Au(111) in normal photoemission spectra. The analysis of the quantum-well binding energies enables one to determine the occupied band of the film material near the band edge. Using these data, the NFE model and the EM model are studied. The surface-state binding energy strongly depends on the image plane location x_i and the band bottom. For calculations of the thickness dependence of the binding energies, however, it is assumed that x_i depends solely on the surface layer of atoms, i.e., x_i is thickness independent. The calculation of x_i itself requires a self-consistent calculation of the surface potential. In our calculations, x_i is fitted by the requirement of reasonable surface-state binding energies of the pure Ag(111) and Au(111) surfaces. The explanation of the different Ag band values obtained from the quantum-well systems Ag/Au(111) and Ag/Cu(111) remains an interesting problem for future investigations.

ACKNOWLEDGMENTS

This work was performed at the Hamburger Synchrotronstrahlungslabor (HASYLAB) at the Deutsches Elektronen-Synchrotron (DESY). The authors wish to thank the HASYLAB staff, especially G. Materlik and R. Reininger for their valuable assistance. Thanks are also due to A. Goldmann for stimulating discussions.

[1]H. Wern, R. Courths, G. Leschik, and S. Hüfner, Z. Phys. B **60**, 293 (1985).
[2]J. G. Nelson *et al.*, Phys. Rev. B **32**, 3465 (1985).
[3]R. Courths, H.-G. Zimmer, A. Goldmann, and H. Saalfeld, Phys. Rev. B **34**, 3577 (1986).
[4]S. D. Kevan and R. H. Gaylord, Phys. Rev. B **36**, 5809 (1987).
[5]T. C. Hsieh and T.-C. Chiang, Surf. Sci. **166**, 554 (1986).
[6]A. P. Shapiro, A. L. Wachs, and T.-C. Chiang, Solid State Commun. **58**, 121 (1986).
[7]T. Miller, A. Samsavar, G. E. Franklin, and T.-C. Chiang, Phys. Rev. Lett. **61**, 1404 (1988).
[8]M. A. Mueller, A. Samsavar, T. Miller, and T.-C. Chiang, Phys. Rev. B **40**, 5845 (1989).
[9]T. Miller, A. Samsavar, M. Mueller, G. Franklin, and T.-C. Chiang, Phys. Scr. **31**, 35 (1990).
[10]K. Meinel, M. Klaua, and H. Bethge, J. Cryst. Growth **89**, 447 (1988).
[11]K. Meinel, M. Klaua, and H. Bethge, Phys. Status Solidi (A) **110**, 189 (1988).
[12]K. Meinel, M. Klaua, and H. Bethge, Ultramicroscopy **20**, 261 (1986).
[13]K. Meinel, M. Klaua, Ch. Ammer, and H. Bethge, Phys. Status Solidi (A) **106**, 493 (1988).
[14]M. G. Goldiner, V. B. Sapoznikov, M. Klaua, and K. Meinel, J. Phys. Condens. Matter **3**, 5479 (1991).
[15]C. A. Feldmann, R. Engelhardt, T. Permien, E.-E. Koch, and V. Saile, Nucl. Instrum. Methods **208**, 785 (1983).
[16]M. Klaua, K. Meinel, and A. Beckmann (unpublished).
[17]F. Garcia-Moliner and J. Rubio, Proc. R. Soc. London Ser. A **324**, 257 (1971).

[18]F. Garcia-Moliner, Ann. Phys. (Paris) **2**, 179 (1977).
[19]R. Perez-Alvarez, H. Rodríguez-Coppola, V. R. Velasco, and F. Garcia-Moliner, J. Phys. C **21**, 2197 (1988).
[20]M. Radny, Surf. Sci. **231**, 43 (1990).
[21]W. Jaskolski, V. R. Velasco, and F. Garcia-Moliner, Phys. Scr. **43**, 337 (1991).
[22]N. V. Smith, Phys. Rev. B **32**, 3549 (1985).
[23]M. Ortuño and P. M. Echenique, Phys. Rev. B **34**, 5199 (1986).
[24]Z. Lenac, M. Sunjic, H. Conrad, and M. F. Kordesch, Phys. Rev. B **36**, 9500 (1987).
[25]S. D. Kevan, Phys. Rev. B **34**, 6713 (1986).
[26]J. Callaway, *Quantum Theory of the Solid State* (Academic, New York, 1976).
[27]R. A. Morrow and K. R. Brownstein, Phys. Rev. B **30**, 678 (1984).
[28]The two poles near the band gap are of physical importance. Only they are taken into account.
[29]G is a continuous function at $x=x'$ because of the symmetries of the wave functions.